Surface Density Measurements for Freely-Propagating Premixed Turbulent Flames at Various Lewis Numbers.

B. Renou, A. Mura, E. Samson and A. Boukhalfa

LAME - CORIA UMR 6614 CNRS
INSA - Avenue de l'Université - BP8
76801 Saint-Etienne-du-Rouvray Cedex
France

Bruno.Renou@coria.fr

INTRODUCTION

In the flamelet conceptual view of turbulent combustion, the reaction zone is analyzed as a collection of laminar flame elements embedded in the turbulent flow [1-2]. One of the major advantages of the laminar flamelet approach is that the complex chemistry calculations are decoupled from the turbulent flow description. As a consequence, the model for the mean reaction rate may be decoupled from the turbulent transport and can be considered as a separate modeling problem. The mean reaction rate can be modeled by the general formulation $\overline{\dot{w}} = Q_k \Sigma$ where Q_k is the local reaction rate per unit flame surface related to the local flame properties integrated along the normal direction to the flame surface, and Σ the flame surface density, i.e., the flame surface area per unit volume [2-3]. The action of the turbulence on the flame surface is described through the flame surface density, whereas chemical effects are included in the local reaction rate. The mean reaction rate averaged along the whole flame surface, $<w>$, can then be expressed with the space averaged fuel burning velocity $<S_C>$, according to the following relation [3]:

$$<w>=\rho_u<S_C>\Sigma \tag{1}$$

where ρ_u is the fresh gas density.

Theory recently provides an exact evolution equation for the flame surface density [4] using the exact definition of the flame surface density function. The flame surface density is then estimated from the conditional gradient of the progress variable c according the following relation:

$$\Sigma\left(C^*,x,t\right)=\overline{\left|\nabla C(x,t)\right|\delta\left(C-C^*(x,t)\right)}=\left[\ \overline{\left|\nabla C\right|_{C*}}\ \right]p(C^*) \tag{2}$$

where $\overline{\left|\nabla C\right|_{C*}}$ is the conditional average of $\left|\nabla C\right|$ for C = C* and p(C*) corresponds to the probability to have C = C* at the given location.

Spatially averaged statistics and flame surface density measurements can be obtained by laser tomography which visualize a planar slice through a premixed flame, enabling the location of the instantaneous position of the flame front in the plane of the laser sheet [5-8]. Furthermore, the Planar Laser Induced Fluorescence technique (PLIF) has been also used to characterize the local flame structure in terms of orientation factors and to evaluate the evolution of flame surface density with the turbulence flow field [9-10].

There is still a lack of experimental results concerning the mean reaction rate or spatial statistics of several turbulent combustion models, in particular for non-stationary premixed turbulent flames and for various Lewis numbers. The local flame structure and the mean stretch evolutions induced by the temporal flame evolution have to take into account the non-stationary effects in these models. Furthermore, the Lewis number effects on the evolutions of spatial statistics are not well known, whereas some numerical simulations have been produced recently [11].

The objectives of the present work concern the characterization of the local flame structure for freely-propagating premixed flames, and the determination of the flame surface density. The influence of the thermodiffusive effects in terms of Lewis number will be also studied.

EXPERIMENTAL SET-UP AND OPTICAL DIAGNOSTICS

The experimental set-up consists in a vertical wind tunnel where the fuel/air mixture is vertically convected into a 80×80 mm square transparency open combustion chamber [12]. The mixtures then pass through a removable turbulence grid and are spark-ignited downstream at the center of the visualization chamber using thin wire electrodes. The produced expanding turbulent flame then propagates upstream in a decaying isotropic turbulence flow. The values of velocity fluctuations observed for both parallel and perpendicular components indicate that the approach flow can be considered as isotropic. Different fuel/air mixtures (propane/air, methane/air and hydrogen/air) have been studied for several equivalence ratio in order to obtain a large range of Lewis numbers ($0.3<Le<1.4$). The combination of the turbulent and chemical reaction enables the influence of parameters such as the ratio u'/S_L, the turbulent length scale and the turbulent Reynolds number Re to be analyzed. These parameters are summarized in Table 1.

In this study, two-dimensional flame front visualizations were obtained by Laser Sheet Tomography. This technique has been adapted to visualize the instantaneous flame front position for several stages of flame propagation, from ignition to fully developed flame in the combustion chamber. The tomographic acquisition system includes a single Nd:YAG 585 pulsed laser with second harmonic generating crystals used to create a Q-switched laser output at 532 nm. The laser sheet is obtained by a combination of spherical-cylindrical lenses with a thickness in the middle of the test sections less than 400µm. The laser sheet with a 75mJ/pulse energy illuminates the flow seeded with micron-sized silicon oil droplets. The position of flame front is determined from the intensity of the light scattered from droplets that evaporate at the entrance of the flame front. The flame front is delineated clearly by the interface separating the fresh gases (light region) from the products (black region). The flame surface images are recorded on CCD camera Micam connected to a frame grabber Euresys Solo, with a spatial resolution of 768 by 512 pixels. A synchronization procedure allows a freely-propagating flame each 30s to be generated and grabbed by the frame grabber. The spatial resolution of the tomographic images was measured at 8 pixels/mm.

IMAGE ANALYSIS

The flame contours are then systematically binarized by using an automatic thresholding procedure based on gray-level histogram thresholding by index of fuzziness [12]. With this procedure, the value of the threshold is adapted to each tomographic recordings and takes into account the seeding and laser light fluctuations during the experiments. Then an edge-finding algorithm is adapted to get a continuous flame edge from each of the images. The detected flame boundaries have been smoothed to remove the noises coming from the digitization steps.

From each set of flame contour, one can obtain the mean progress variable distribution across the flame front for all the experimental conditions and propagation times. All the instantaneous flame front images are centered on their geometric center, to remove cycle to cycle fluctuations of flame front position on the laboratory reference. Individual flame contours represent the instantaneous map of the progress variable while averaging the flame contours provides the mean progress variable distribution, giving a map of the probability of presence of flame front. The two-dimensional <C> distribution converges towards concentric circles indicating that the <C> distribution can be assumed to be mono-dimensional (Figs. 1 and 2) . The shape of this distribution slightly depends on the number of flames and converges towards a mean value for 150 flames.

EXPERIMENTAL RESULTS

The flame surface density can be directly obtained from tomographic recordings by using either the exact geometrical expression (Eq. 2) or by the algebraic expression deduced from the BMCL model [13]. Here, the method deduced from Eq. 2 is used with 150 flames for each propagation time. The temporal evolutions of flame surface density determined for an hydrogen/air mixture are displayed in Fig. 3.

• As we can observe, the global profiles are symmetrical about a peak value and globally present a parabolic trend as expected from the BMCL model [13]. They are comparable in shape to those found by Veynante et al. [14] in two dimensional V-flames and Deschamps et al. [9], in SI-engines.

• Furthermore, the maximum of flame surface density, noted Σ_{max}, decreases as the flame propagates, according to a logarithmic trend. This evolution has also been observed by direct numerical simulation on 2D cylindrical flames [16]. The decreasing of the flame surface density distribution as the flame propagates can be explained by the geometrical definition of the flame surface density given by Cant et al. [14, 17]:

$$\Sigma = \frac{-1}{M_i} \nabla \langle C \rangle \qquad (3)$$

where M_i are the mean part of the components of the normal vector **n** to the local flame surface. For propagation times varying from 3ms to 8ms, the slopes of <C> versus the flame radius decrease (Fig. 2), which leads consequently to a decreasing of the maximum of the flame surface density as the flame propagates. The influence of propagation time on <C> profiles is governed by transient process of flame kernel. Indeed, the kernel is initially quasi-laminar, and as it grows in size, the range of activate scales contributing to its wrinkling grows accordingly [12].

• The influence of the Lewis number is not found in the temporal evolution of flame surface density profiles in our range of Lewis numbers. Indeed, the temporal evolution of the maximum flame surface density Σ_{max} is reported in Fig. 4, at quasi-constant values of u'/S_L. The evolutions of Σ_{max} are identical for all the Lewis numbers used in this experimental work, for two levels of turbulence. This result is confirmed by 3D direct numerical simulations where the Σ-profiles obtained for Lewis numbers of 1.2, 1.0 and 0.8 are identical in <C>-space [11]. This result indicates that the effect of the Lewis number on the flame surface density, as observed in these experimental results, is primarily an effect on turbulent flame thickness δ_T. Indeed, the influence of the thermodiffusive effects on flame wrinkling structure can be pointed out by way of turbulent flame thickness deduced from <C> gradient across the flame front [18] (Fig. 5). For hydrogen/air flames, this behavior is enhanced in comparison with methane and propane, in accordance with similar results concerning the local and mean spatial flame front characteristics evolution obtained by high speed laser tomography [12].

• In the flamelet model point of view, the influence of the turbulence level on the mean reaction rate is described through the flame surface density. Consequently, the role of the turbulence on the flame surface density is expected to be crucial and non-negligible.
Several numerical and experimental concerning the influence of u'/S_L on Σ_{max} are available in literature and present some opposite evolutions. An experimental work has been conducted for turbulent Bunsen flames, and for a large range of u'/S_L values [15]. The decreasing of Σ_{max} with u'/S_L is lower than our experimental results, but the trend is similar. Furthermore, the numerical simulation of Echekki et al. [16], on 2D cylindrical flames, also indicates a decreasing of Σ_{max} with an increasing of the turbulence level. Choi and Huh [19] have compared several closure models for the transport equation of Σ and have found an increasing of Σ_{max} with u'/S_L.
In our experimental configuration and within experimental uncertainties, the maximum flame surface density presents a slight influence with u'/S_L, for the three fuel/air mixtures used in this work (Fig. 6). For each propagation time, Σ_{max} decreases for an increasing of the turbulence level u'/S_L (at constant laminar flame speed S_L), whatever the variation of the integral length scale L_0. This difference on Σ_{max}

also decreases as the flame propagates and seems to converge towards a value independent of the level of turbulence u'/S_L. This supposition should have to be confirmed and validated by a new set of experiments for propagation times higher than two or three integral time scale of turbulence τ_T.

REFERENCES

1. Williams, F.A., in *Combustion Theory* (2nd ed) The Benjamin/Cummings Publishing Company, Inc., (1985), pp. 415-423.
2. Marble, F.E., and Broadwell, J.E., (1977), Project Squid Report, TRW-9PU, Purdue University West, Lafayett, Indiana.
3. Poinsot, T.J., Candel, S., and Trouvé, A., *Prog. Energy Combust. Sci.* 21:531-576, (1996).
4. Pope, S.B., *Int. J. Engng Sci.* 26 :445-469, (1988).
5. Chew, T.C., Britter, R.E., and Bray, K.N.C., *Combust. Flame*, 80:65-82, (1990).
6. Deschamps B.M., Smalwood G.J., Prieur J., Snelling D.R. and Gülder Ö.L., (1996), *Twenty–Sixth Symposium (International) on Combustion, The Combustion Institute*, pp. 427-435.
7. Shy, S.S, Lee, E.I., Chang, N.W., and Yang, S.I., (2000), *Twenty-Eight Symposium (International) on Combustion,* The Combustion Institute, Pittsburgh, PA.
8. Knaus, D.A., and Gouldin, F.C., (2000), *Twenty-Eight Symposium (International) on Combustion,* The Combustion Institute, Pittsburgh, PA, paper 5A08.
9. Smallwood, G.J., and Deschamps, B.M., SAE Fuels & Lubricants Technical Papers, SAE 962088, (1996).
10. Lee, G.G., Huh, K.Y., and Kobayashi, H., *Combust. Flame* 122:43-57, (2000).
11. Trouvé, A., and Poinsot, T., *Jour. Fluid Mech.* 118:537-557, (1994).
12. Renou, B., Boukhalfa, A., Puechberty, D., and Trinité, M., *Combust. Flame*, 123:507-521, (2000).
13. Bray K.N.C., Champion M. and Libby P.A., (1989), In R. Borghi and S. Murphy (Eds.), *Turbulent Reacting Flows*, Volume 40 of Lecture Notes in Engineering, pp. 541-563, Springer.
14. Veynante D., Duclos J.M. and Piana J., (1994), *Twenty–Fivth Symposium (International) on Combustion, The Combustion Institute*, pp. 1249-1256.
15. Smallwood, G.J., Snelling, D.R., and Gülder, Ö.L., (1999), *17th ICDERS,* Heidelberg, Germany, paper 190.
16. Echekki T., Poinsot T.J., Baritaud T. and Baum M. (1996), In T. Baritaud, T. Poinsot and M. Baum (Eds.), *Direct Numerical simulation for turbulent reacting flow*, pp. 123-145, Technip Edition.
17. Cant R.S., Pope S.B. and Bray K.N.C., (1990), *Twenty–Third Symposium (International) on Combustion, The Combustion Institute*, pp. 809-815.
18. Namazian, M., Shepherd, I.G., and Talbot, L., *Combust. Flame* 64:299-308, (1986).
19. Choi, C.R., and Huh, K.Y., *Combust. Flame*, 114:336-348, (1998).

LIST OF TABLE AND FIGURES

Fuel/air mixture	u' (m/s)	L_0 (mm)	τ_T (ms)	Φ	S_L^o (m/s)	u'/S_L^o	Re_T	Da	Ka	Le
C_3H_8/air	0.34	6.5	19.1	1.00	0.400	**0.85**	146	78	0.09	1.40
CH_4/air	0.34	6.5	19.1	1.00	0.370	**0.92**	146	60	0.11	1.01
H_2/air	0.18	3.0	16.7	0.27	0.180	**1.00**	36	11	0.29	0.33
C_3H_8/air	0.51	6.0	11.8	1.00	0.400	**1.28**	202	48	0.18	1.40
CH_4/air	0.51	6.0	11.8	1.00	0.370	**1.38**	202	26	0.31	1.01
H_2/air	0.34	6.5	19.1	0.27	0.180	**1.89**	146	13	0.51	0.33

Table 1 : Experimental conditions

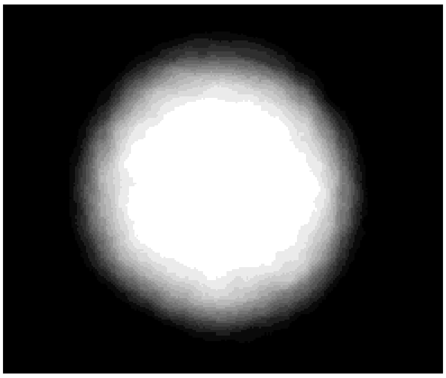

Fig. 1 : Two-dimensional field of <C>, for 150 methane/air flames (u'/S_L=1.38).

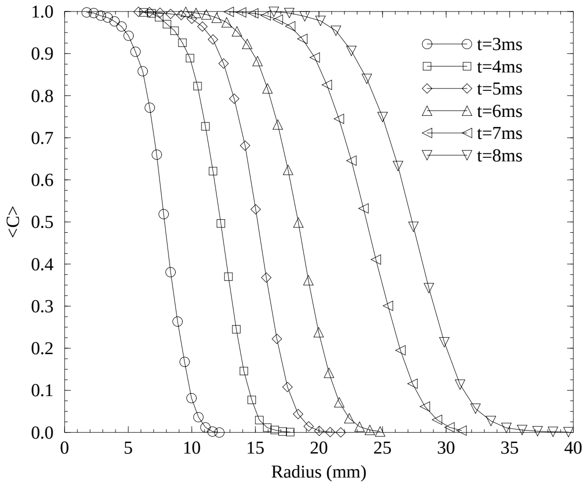

Fig. 2 : Temporal evolution of <C> distribution for turbulent propane/air flame (u'/S_L= 1.28)

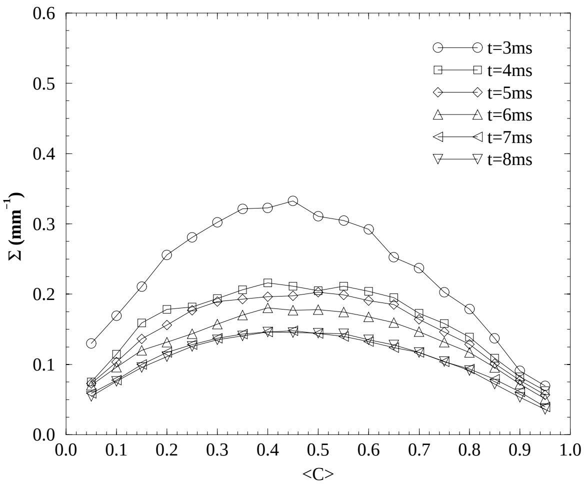

Fig. 3: Temporal evolution of the flame surface density for hydrogen/air flames, u'/S_L=1.89.

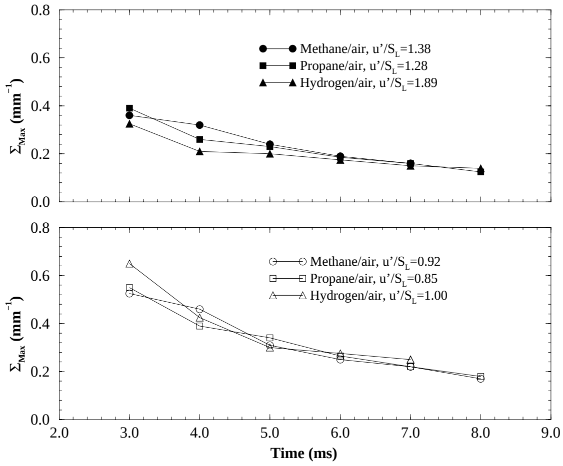

Fig.4: Temporal evolution of Σ_{max} for various Lewis numbers

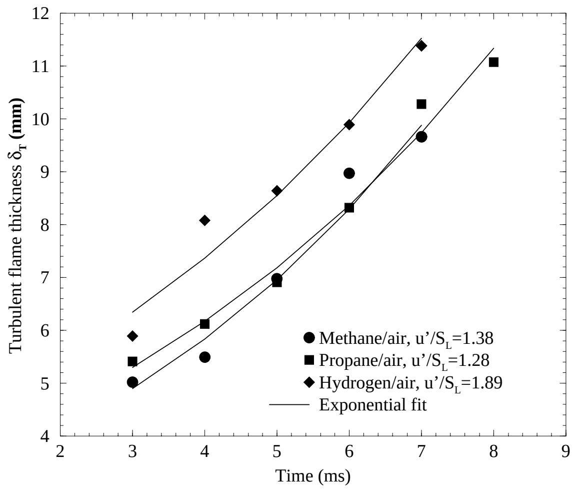

Fig. 5 : Temporal evolution of the turbulent flame thickness δ_T.

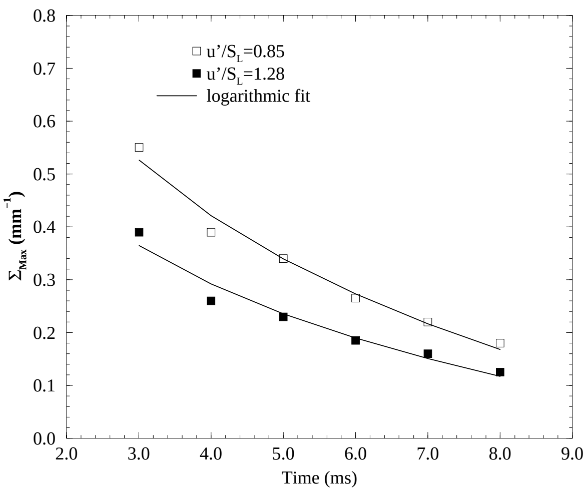

Fig. 6: Temporal evolution of the maximum of the flame surface density for propane/air flame.